Off-design and Part-load Assessment of an Exergy-optimized Organic Rankine Cycle for low to medium Waste Heat Temperatures

José Mota, Márcio Santos, Joel Morgado, Eduardo Ribeiro and José Ribeiro*

University of Coimbra, ADAI-LAETA, Department Mechanical Engineering, Rua Luís Reis Santos, Pólo II, 3030-788 Coimbra, Portugal
**Corresponding Author: jose.mota@dem.uc.pt*

Abstract:

This work presents a detailed off-design model of an organic Rankine cycle system for industrial waste heat recovery and compares its performance with the corresponding design-point configuration. The design point is determined by maximizing exergy efficiency under specified boundary conditions, assuming fixed isentropic efficiencies and neglecting heat and pressure losses. In contrast, the off-design model includes component-level modelling of the pump, expander, condenser, and evaporator in MATLAB, enabling a realistic representation of system behaviour under part-load conditions. The heat source temperature is varied over a low-to-medium range to assess part-load performance. The system operates considering Paratherm™ HE as the thermal energy source and water as the cold sink, while R1234ze(E) is selected as the working fluid. The results show that the off-design model predicts the performance parameters of the design model with acceptable accuracy. However, they also highlight the need for ORC systems to be specifically tailored to given heat source conditions, as a significant performance degradation is observed when operating conditions deviate substantially from the design point. The component responsible for the operational bottleneck was identified, with the evaporator emerging as the primary limiting element.

Keywords:

Organic Rankine Cycle; Heat Recovery; Off-design modelling; Part-load assessment

1. Introduction

Significant efforts have been devoted in recent years to the development of more sustainable electricity generation technologies, driven by increasing environmental concerns and decarbonization targets. One of such technologies are waste heat recovery (WHR) systems for power generation, which can enhance the efficiency and energy self-sufficiency of industrial processes while reducing CO_2 emissions [1]. Among the available technologies, the Organic Rankine Cycle (ORC) has emerged as a mature and promising solution [2–5], as evidenced by its steadily increasing installed capacity. In fact, there has been considerable investment in ORC installations by established manufacturers such as Turboden and ORMAT, alongside the emergence of new companies specializing in this technology, such as Climeon and TICA, which further highlights the growing relevance of ORC as a heat-to-power conversion technology [6]. Despite its proven maturity and reliability at higher power capacities (>1000 kW), micro- and small-scale WHR–ORC systems still require further development and performance validation under off-design conditions to ensure their technical viability.

In an effort to develop a fully predictive performance model of a micro combined heat and power ORC system, Santos et. al [7] proposed dedicated sub-models for each system component, followed by a closure procedure to ensure convergence of the overall model. Using R245fa as the working fluid, the model was experimentally validated, showing prediction errors below 10%. Motivated by the fact that many studies assume fixed component performance, particularly for heat exchangers and expanders under off-design conditions, Chatzopoulou et al. [8] modelled two configurations for both the condenser and evaporator, as well as two types of volumetric expanders. The ORC performance was subsequently optimized for part-load operation of a stationary internal combustion engine. Considering both technical and economic aspects, in [9] the ORC performance under off-design conditions was evaluated by varying the mass flow rates and inlet temperatures of the heat source and sink, as well as the degrees of superheating and subcooling and the pump rotational speed. The heat exchangers were modelled using the logarithmic mean temperature difference (LMTD) method, with the required heat transfer area calculated accordingly and the expander performance was

determined using correlations based on experimental data. To overcome the dependency on experimental data for volumetric expander modeling, the work developed in [5] extended the semi-empirical model proposed by [10] to accommodate different working fluids and scroll expander geometries. The adapted model facilitates the design process and enables the prediction of off-design performance with acceptable accuracy.
In the present work, dedicated sub-models are developed for each ORC component. These sub-models are designed to accurately predict the performance of a pre-selected pump, scroll expander, evaporator and condenser, chosen based on a specified design operating point. The individual sub-models are then integrated into a comprehensive system model, ensuring full thermodynamic closure of the cycle. By varying the heat source conditions, part-load performance is evaluated and compared with design point operation. Since each component operates within specific capacity limits defined by its boundary conditions, the component responsible for operational bottlenecks is identified for each set of input conditions. This approach enables the assessment of potential oversizing requirements, ensuring ORC suitability under highly variable heat source conditions.

2. System Description

The ORC is a heat to power conversion technology derived from the Clausius Rankine cycle. In contrast to conventional systems that employ water as the working fluid, the ORC utilizes organic fluids, such as hydrofluoroolefin refrigerants. These fluids exhibit significantly lower boiling temperatures and operating pressures, enabling efficient energy conversion from low to medium temperature heat sources.
The ORC system comprises four main components: i) expander, ii) pump, iii) evaporator, and iv) condenser. The selected components are described in Table 1.

Table 1. *List of the selected components*

Component	Type	Model	Manufacturer
Expander	Volumetric - Scroll	ZR310	Copeland®
Pump	Centrifugal - Vertical multistage	CR 3-21 A-A-A-E-HQQE	Grundfos®
Evaporator	Plate heat exchanger - Brazed	B250ASHx116/1P-NC-H	SWEP
Condenser		B400THx180/1P-SC-S	

The expander is a key component of the ORC system, responsible for converting the thermal energy of the working fluid into mechanical power. In the present study, an inverted scroll compressor is employed as the expansion device. Scroll compressors are particularly suitable for this application due to their robust design, relatively high isentropic efficiency, and good performance under variable operating conditions.
The conversion of a scroll compressor into an expander involves reversing its operation, allowing high pressure vapor to expand through the scroll mechanism and produce shaft work. This approach has been widely investigated as a cost-effective alternative to purpose-built expanders, especially in small scale ORC systems. Previous studies have demonstrated the feasibility and performance of such modifications. For instance, works such as [10], [11], and [12] analysed the use of scroll compressors operating as expanders in ORC applications, highlighting their reliability and favourable efficiency in low to medium power ranges.
The pump is responsible for increasing the pressure of the working fluid from condenser to evaporator conditions, ensuring continuous circulation within the ORC loop. This unit is a vertical multistage centrifugal pump with inline suction and discharge ports, meaning both connections are positioned at the same elevation. This configuration facilitates compact system integration and simplifies piping layout. The multistage design enables the pump to achieve the required pressure rise while maintaining stable operation, with a maximum efficiency of about 60%. Such pumps are commonly employed in ORC systems due to their reliability, ability to handle moderate flow rates, and suitability for continuous operation under steady state conditions. The selected model meets the operational requirements of the system, particularly in terms of pressure increase and compatibility with the working fluid.
Brazed plate heat exchangers (BPHE) consist of a series of corrugated metal plates, typically made of stainless steel, which are brazed together to form a compact and highly efficient heat transfer device.
One of the main advantages of BPHEs is their high-power density, attributed mainly to the corrugation pattern in each plate, which promotes turbulence, resulting in high heat transfer coefficients. This compactness is particularly advantageous in ORC applications, where system integration and space constraints are often relevant. Furthermore, BPHEs exhibit low refrigerant charge requirements, which is beneficial when using organic working fluids, both from an economic and environmental perspective.
In ORC systems, BPHEs are widely used for both evaporation and condensation processes due to their ability to handle phase change efficiently. Moreover, their modular design and relatively low cost make them an attractive option compared to shell and tube heat exchangers, particularly in small to medium scale installations.

The selected models were chosen based on their thermal performance, compatibility with the working fluid, and ability to meet the required heat duty of the design point conditions, considering the characteristics of the heat source from a particular case study.

3. Methodology

In order to evaluate the part-load performance of the designed ORC model, both the heat source mass flow rate, $\dot{m}_{HS}$, and inlet temperature, $T_{HS,in}$, were varied within the low-to-medium temperature range. The results were obtained through a simulation process, in which each component was modelled in MATLAB, and the CoolProp database was used to determine the thermodynamic properties of the working fluids.

3.1. Design-point model

The design-point model was based on specific heat source characteristics from a case study, where the available mass flow rate and temperature are 1.1 kg/s and 135 ºC, respectively. Aiming for full heat recovery, and considering a minimum outlet temperature of 60 ºC, the working fluid R1234ze(E) was selected. Its T–s diagram along the ORC is presented in Figure 1.

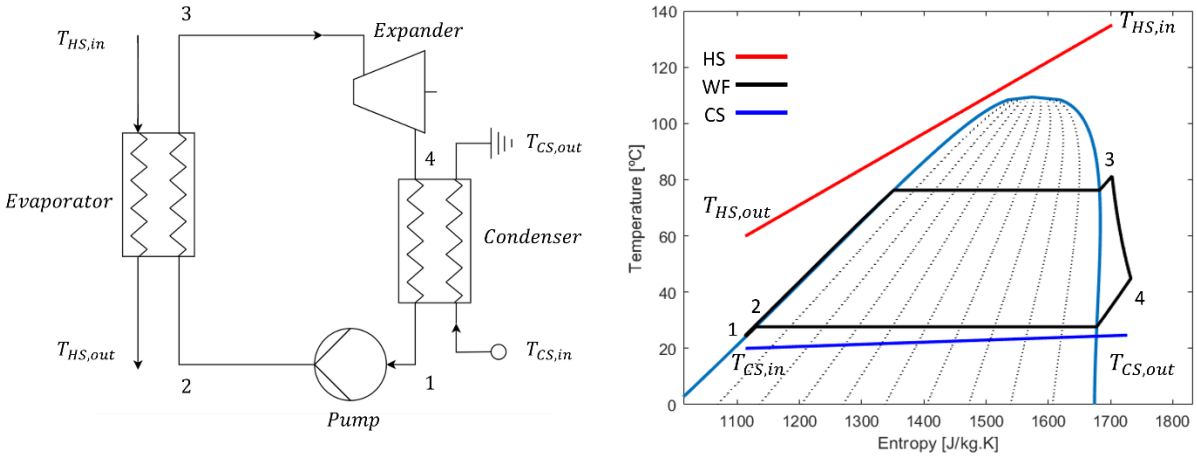

Figure. 1. *a) Schematic of the ORC, b) T-s diagram of R1234ze(E) for the design-point conditions.*

The operating parameters obtained from the design-point model are listed in Table 2, while the corresponding performance outputs, used for comparison with off-design and part-load conditions, are presented in Table 3.

Table 2. *Operation parameters for the design point*

$\dot{m}_{HS}$ (kg/s)	$T_{HS,in}$ (ºC)	$\dot{m}_{WF}$(kg/s)	p_{evap} (bar)	p_{cond} (bar)	ΔT_{SH} (ºC)	$\eta_{is,exp}$ (%)
1.1	135	0.72	18.5	5.4	5	60

Table 3. *List of outputs for the design point*

$\dot{Q}_{evap}$(kW)	RP (−)	η_{ex} (%)	η_{th} (%)
144.2	3.43	27.88	7.50

Subcooling and superheating degrees of 3.5 ºC and 5 ºC, respectively, were selected to prevent pump cavitation and the expansion of a two-phase working fluid. A pressure ratio, RP, of 3.43 is considered acceptable, as excessively high pressure ratios limit the use of scroll expanders due to volumetric ratio constraints inherent to their operating principle. By neglecting heat and pressure losses and assuming a fixed expander isentropic efficiency of 60% and a pump isentropic efficiency of 98%, the design model predicts a recovered thermal power of 144 kW, with exergy and thermal efficiencies of 27.88% and 7.50%, respectively.

3.2. Off-design model

To provide a more realistic representation of ORC performance, dedicated sub-models were developed for each individual component. Based on the component selection described in Chapter 2, the pump, expander, evaporator, and condenser were modelled independently using different approaches. Iterative loops were implemented to ensure convergence and achieve complete thermodynamic closure of the cycle.

3.2.1. Pump sub-model

The pump was the simplest component to model. Based on the manufacturer's performance curves, presented in Figure 2, an interpolation procedure was applied to determine the evaporating pressure, p_{evap}, isentropic efficiency, $\eta_{is,pump}$, outlet temperature at state point 2, T_2, and the power consumption of the pump, $\dot{W}_{pump}$. The boundary conditions for this component are defined by the manufacturer and include the minimum and maximum working fluid mass flow rates, as well as the maximum operating pressure.

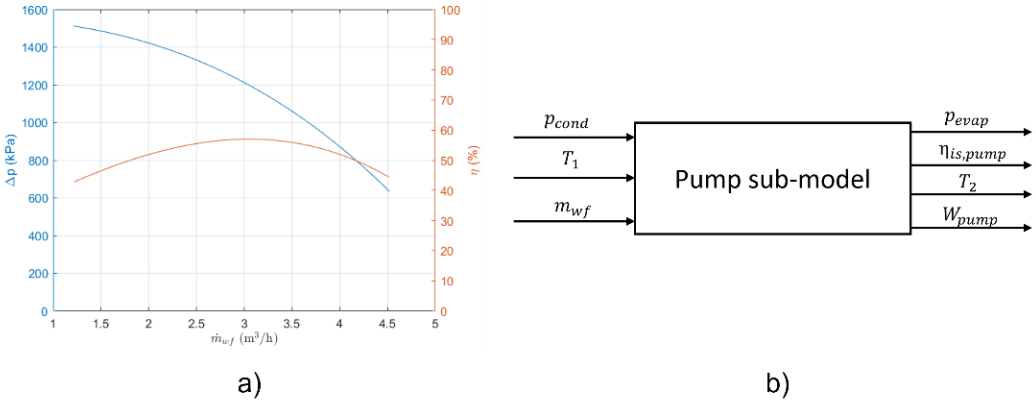

Figure. 2. *a) Pump performance curves for pressure difference and efficiency, b) List of inputs and outputs of the pump sub-model.*

3.2.2. Expander sub-model

The expander sub-model is based on the semi-empirical model developed in [11], illustrated in Figure 3. This model accounts for both internal heat transfer between the working fluid and expander components, and external heat transfer with the surroundings. By considering the geometric characteristics of the selected scroll expander, Exp_{geom}, along with the inlet temperature, T_3, inlet and outlet pressures, p_{evap} and p_{cond}, and rotational speed, N_{rot}, the model predicts the working fluid mass flow rate, $\dot{m}_{WF}$, outlet temperature, T_4, isentropic efficiency, $\eta_{is,exp}$, and generated electrical power, P_{elect}.

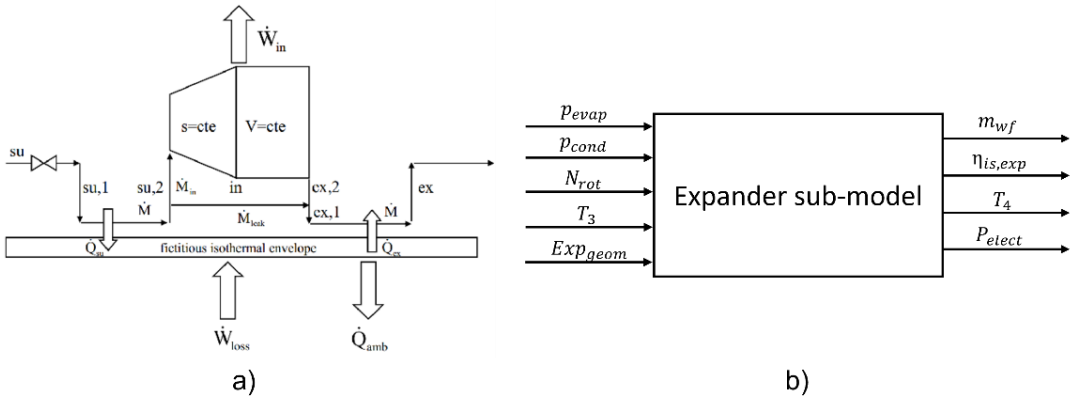

Figure. 3. *a) Schematic of the expander sub-model developed by Lemort et al. [11]), b) List of inputs and outputs for the expander sub-model.*

The boundary conditions for the expander are primarily associated with its geometry, particularly the built-in volume ratio, which is directly related to the maximum allowable pressure ratio. Additionally, operational limits on rotational speed are considered, ranging from 500 to 3500 rpm.

3.2.3. Condenser and Evaporator sub-models

Both heat exchangers were modelled using the logarithmic mean temperature difference (LMTD) method. Different heat transfer correlations were applied for each phase and fluid stream to estimate the convective heat transfer coefficients, being presented in Table 4. For single-phase heat transfer of the working fluid, the Martin correlation [13] was employed, as it has been shown by Dickes et al. [14] to provide accurate predictions for BPHEs. This correlation was also applied to the heat source and cold sink streams across all single-phase regions. For phase-change processes, specific correlations were used. The condensation process of the working fluid was modelled using the correlation proposed by Han et al. [15], following the approach adopted by Santos et al. [7]. Similarly, the evaporation process was modelled using the boiling correlation from Han et al. [16].

Table 4. *Heat transfer correlations for the off-design model*

Heat transfer region	Fluid	Correlation	Author
Single phase (liquid or vapour)	Heat source Cold sink Working fluid	$Nu = 0.205 \cdot Pr^{\frac{1}{3}}(f \cdot Re^2 \cdot \sin(2\beta))^{0.374}$ $\frac{1}{\sqrt{f}} = \frac{\cos(\beta)}{\sqrt{0.045 \cdot \tan(\beta) + 0.09 \cdot \sin(\beta) + \frac{f_0}{\cos(\beta)}}}$ $f_0 = \begin{cases} \frac{16}{Re}; Re \leq 2000 \\ (1.56 \cdot \ln(Re - 3)^2; Re > 2 \end{cases}$	Martin [13]
Two-phase (evaporation)	Working fluid	$Nu = C_1 \cdot Re^{C_2} \cdot Bo^{0.3} \cdot Pr^{0.4}$ $C_1 = 2.81(\frac{P_C}{D_h})^{-0.041} \cdot \beta^{-2.83}$ $C_2 = 0.746(\frac{P_C}{D_h})^{-0.082} \cdot \beta^{0.61}$	Han et al. [16]
Two-phase (condensation)	Working fluid	$Nu = C_1 \cdot Re^{C_2} \cdot Pr^{\frac{1}{3}}$ $C_1 = 11.22(\frac{P_C}{D_h})^{-2.83} \cdot (\frac{\pi}{2} - \beta)^{-4.5}$ $C_2 = 0.35(\frac{P_C}{D_h})^{0.23} \cdot (\frac{\pi}{2} - \beta)^{1.48}$	Han et al. [15]

Since these correlations depend on geometric parameters that are not disclosed by manufacturers, such as the hydraulic diameter, D_h, corrugation pitch, P_C, and Chevron angle, β, a reverse engineering approach was adopted. Manufacturer-provided design-point data was used to estimate these parameters.

The hydraulic diameter is given by Equation 1 as defined in [17] where b is the flow channel gap and φ is the enlargement factor and is defined as the ratio between the effective and projected areas.

$$D_h = \frac{2*b}{\varphi} \quad (1)$$

The channel gap was determined using the channel velocity provided by the manufacturer under design-point conditions, which is given by Equation 2.

$$v_{ch} = \frac{\dot{m}_{WF}}{\rho_{WF} * A_{ch}} \quad (2)$$

Where ρ_{WF} is the working fluid density and A_{ch} is the total channel flow area, defined by Equation 3.

$$A_{ch} = \frac{b*(N_{pl}-1)}{2*L_w} \quad (3)$$

With N_{pl} being the total number of plates and L_w the effective plate width of the heat exchanger. In this way, by knowing the channel velocity at a given point, the flow channel gap can be calculated. As for the enlargement factor, this was calculated considering the effective area, A_{eff}, which is also given by the manufacturer, and the projected area, which can be defined as by Equation 4.

$$A_{proj} = L_w * L_p * N_{pl} \quad (4)$$

Where L_p is the effective plate length of the heat exchanger. To determine the corrugation pitch and Chevron angle for both the evaporator and condenser, a parameter sweep procedure was performed. For given inlet temperatures and pressures at the design point, outlet temperatures were calculated for different combinations of P_C and β. These results were then compared with manufacturer-provided outlet temperatures. The values of P_C and β that yielded the best agreement were selected, as illustrated in Figure 4.

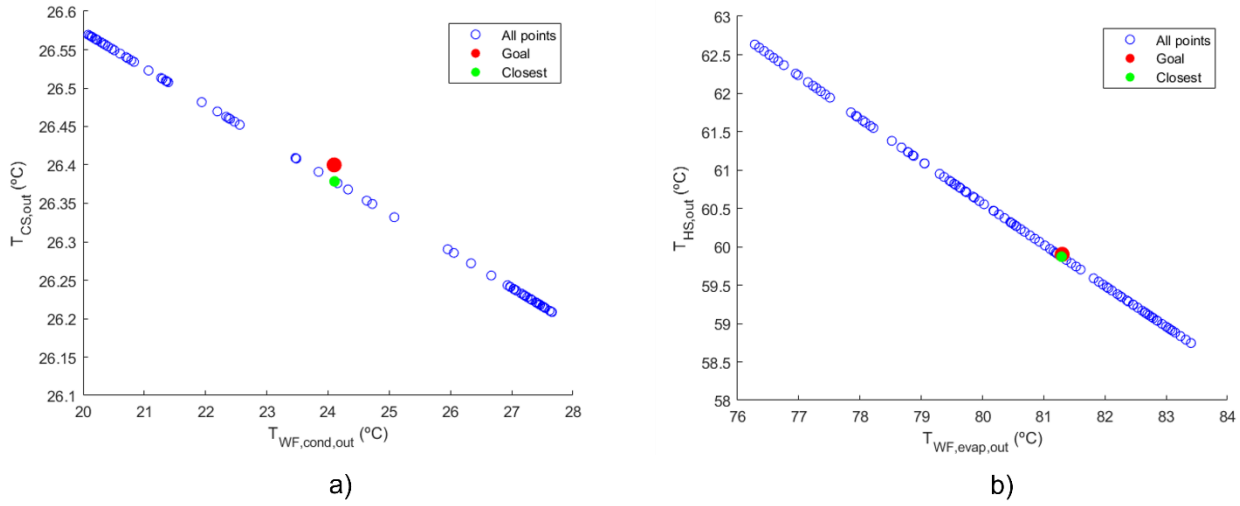

Figure. 4. *Determination of the corrugation pitch and Chevron angle for: a) condenser, b) evaporator.*

Having estimated all of the unknown geometric parameters of the heat exchangers, the evaporator and condenser sub-models were developed, being depicted in Figure 5.

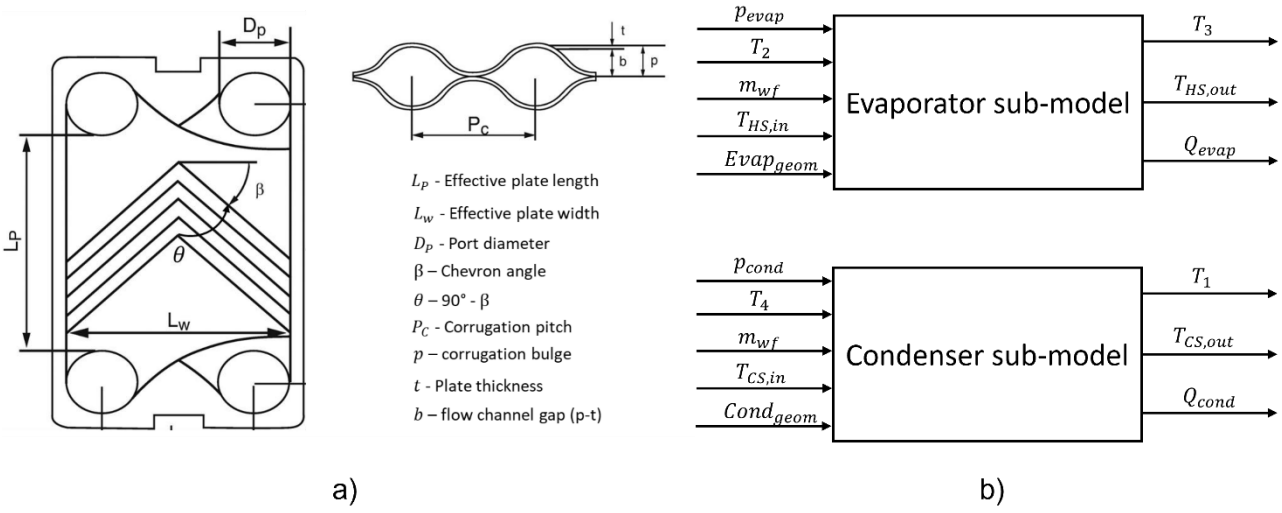

Figure. 5. *a) Schematic of the BPHE (adapted from [18]) b) List of inputs and outputs for the evaporator and condenser sub-models.*

3.3. Additional Considerations

The heat transfer fluid Paratherm™ is considered as the heat source for the modelled ORC. The inlet temperature and mass flow rate are varied from 100-140 ºC and 0.5-1.3 kg/s, respectively, and a minimum $T_{HS,out}$ of 60 ºC is defined. The cold sink considered is water, having an inlet temperature in the condenser of 20 ºC and a mass flow rate of 5 kg/s. For each combination of heat source inlet conditions, the working fluid mass flow rate, $\dot{m}_{WF,i}$, and condensation pressure, $p_{cond,j}$, are varied across a wide range to determine the operation parameters that maximize exergy efficiency, given by Equation 5.

$$\eta_{ex} = \frac{\dot{W}_{net}}{\dot{E}_{in}} \qquad (5)$$

Where $\dot{W}_{net}$ is defined as the net work output, being the difference between the mechanical work produced by the expander and the mechanical work consumed by the pump and $\dot{E}_{in}$ is the exergy flow rate of the heat source, which is defined by Equation 6.

$$\dot{E}_{in} = \dot{m}_{HS} * [(h_{HS,in}\text{-}h_{HS,0})\text{-}T_0 * (s_{HS,in}\text{-}s_{HS,0})] \qquad (6)$$

Where $h_{HS,in}$ and $s_{HS,0}$ are the specific enthalpy and entropy of the heat source at inlet conditions, while subscript 0 refers to a reference state, considerend as 25ºC and 1 atm.

Apart from the exergy efficiency, the thermodynamic efficiency was also determined, which is defined by:

$$\eta_{th} = \frac{\dot{W}_{net}}{\dot{Q}_{evap}} \qquad (7)$$

With $\dot{Q}_{evap}$ being the supplied thermal power to the working fluid in the evaporator.

The integrated ORC model begins with the condenser sub-model, initiating a value of the working fluid inlet temperature in the condenser, $T_{4,init}$. The model then runs in the following order: condenser → pump → evaporator → expander. An initial value of the rotational speed of the expander, $N_{rot,init}$, is given, and an iterative process occurs in order to determine N_{rot} that results in a mass flow rate equal to $\dot{m}_{WF,i}$. The outlet expander temperature, T_4, is then compared to $T_{4,init}$ until full closure of the cycle is achieved.

4. Results and Discussion

A total of 81 different $\dot{m}_{HS}$ and $T_{HS,in}$ combinations were tested. Considering the variation range of the $\dot{m}_{WF}$ and p_{cond}, a total of 46,656 possible combinations were simulated. For each $\dot{m}_{HS}$-T_{HS} pair, the maximum obtained exergy efficiency was selected and the respective outputs were compared with the ones from the design point. Starting with Figure 6, the maximum exergy and respective thermodynamic efficiencies for each $\dot{m}_{HS}$-T_{HS} pair is presented.

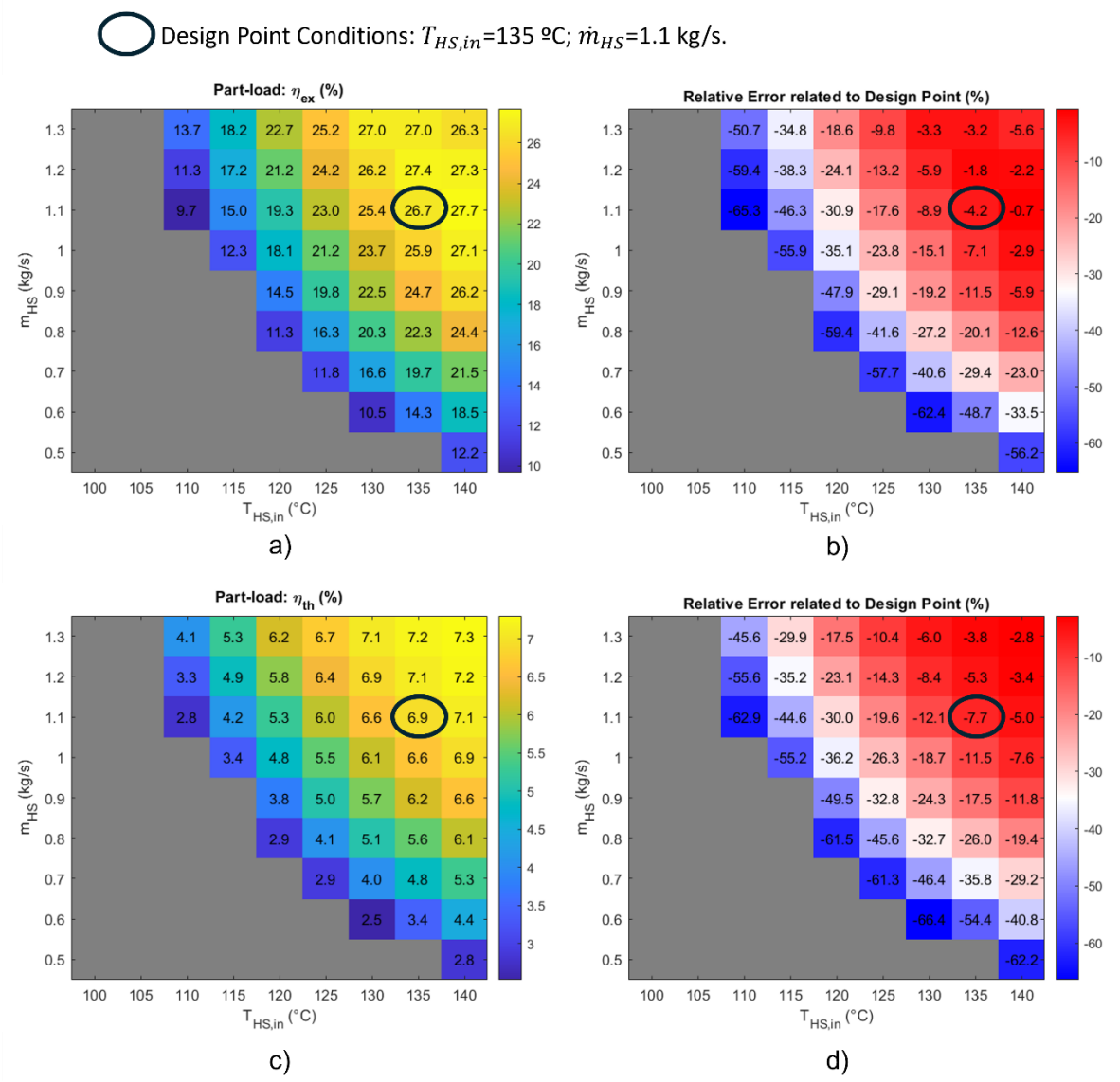

Figure. 6. *a) Part-load assessment of η_{ex}, b) Relative error of η_{ex} to the design-point, c) Part-load assessment of η_{th}, b) Relative error of η_{th} to the design-point.*

Considering that the design point corresponds to a heat source mass flow rate, $\dot{m}_{HS}$, of 1.1 kg/s and an inlet temperature, $T_{HS,in}$, of 135 ºC, the off-design model predicts exergy and thermal efficiencies of 26.7% and 6.9%, respectively. These values represent reductions of 4.2% and 8.0% when compared to the design-point conditions. As the available heat decreases, both qualitatively, in terms of temperature, and quantitatively, in terms of mass flow rate, this performance degradation becomes more pronounced, with reductions of up to 65.2% in exergy efficiency and 66.7% in thermal efficiency.

The grey region indicates operating conditions for which the current model, considering the previously selected components, is unable to ensure feasible ORC operation. Out of the 81 tested combinations of $\dot{m}_{HS}$ and $T_{HS,in}$,

only 45 resulted in successful electricity generation. The infeasible cases arise either from violations of component boundary conditions or from the inability of one or more components to operate under the specified conditions.

For instance, when the heat source inlet temperature falls below 110 ºC, no admissible solution is obtained, regardless of the combination of $\dot{m}_{WF}$, and p_{cond}. The root cause of infeasibility depends on the interaction between $\dot{m}_{WF}$, p_{cond}, and $T_{HS,in}$, as illustrated in Figure 7.

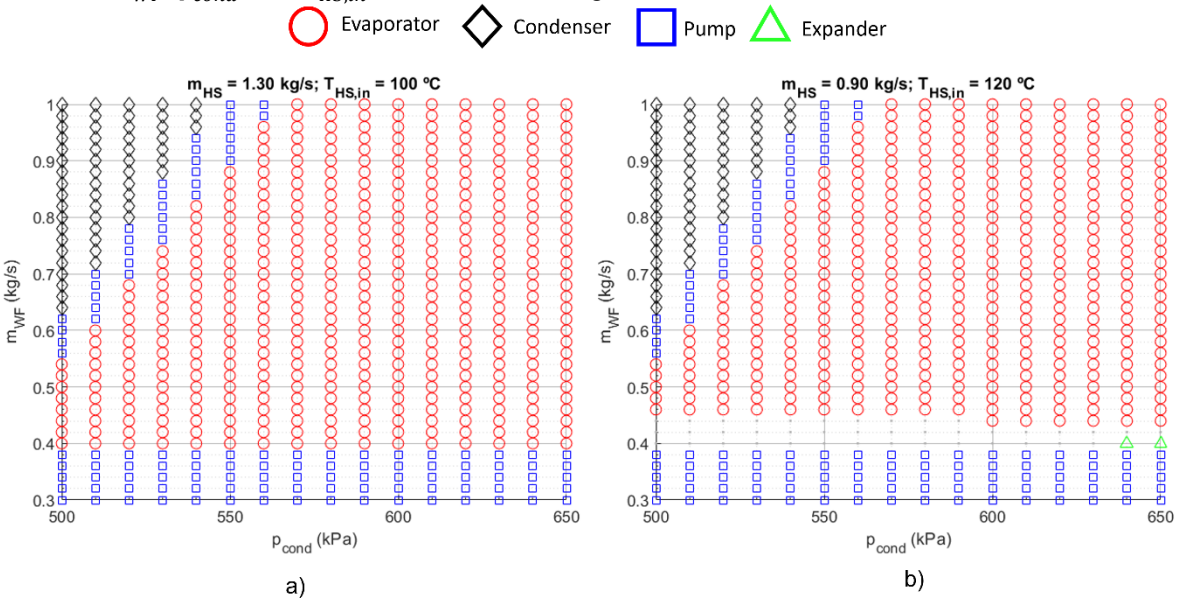

Figure. 7. *Responsible component for the bottleneck effect for: a) $\dot{m}_{HS}$=1.3 kg/s and $T_{HS,in}$=100 ºC, b) $\dot{m}_{HS}$=0.9 kg/s and $T_{HS,in}$=120 ºC.*

In Figure 7 a), corresponding to a lower heat source inlet temperature, no combination of $\dot{m}_{WF}$ and p_{cond} allows full ORC operation. At low condensation pressures and high working fluid mass flow rates, the condenser becomes the limiting component. A decrease in condensation pressure reduces the saturation temperature of the working fluid, thereby lowering the LMTD. Simultaneously, higher $\dot{m}_{WF}$ increases the heat transfer demand. The combination of these effects results in insufficient heat transfer area in the selected condenser to meet the required thermal load, preventing proper cycle operation.

When the pump acts as the limiting component, this is due to constraints on the minimum and maximum allowable volumetric flow rates. For given values of $\dot{m}_{WF}$and p_{cond}, the resulting volumetric flow rate may fall outside the operational range specified for the selected pump, thereby invalidating the operating condition.

For the remaining infeasible cases, the evaporator is responsible for the operational bottleneck. Although increasing the condensation pressure and reducing $\dot{m}_{WF}$ can alleviate constraints in the condenser and pump, the evaporator is unable to deliver the required heat transfer at lower heat source inlet temperatures. This limitation persists across all tested heat source mass flow rates, highlighting the dominant influence of temperature as the primary restricting factor.

Analysis of Figure 7 b) reveals a similar overall trend; however, the expander also emerges as a limiting component under certain conditions, and a subset of admissible operating points is observed. Within a specific range of working fluid mass flow rates, the ORC can operate across nearly all condensation pressures. However, increasing $\dot{m}_{WF}$ beyond this range leads to insufficient heat transfer in the evaporator, while decreasing it results in expander rotational speeds below 500 rpm, violating the minimum operational limit of this component, or the resulting volumetric flow rate falls outside the admissible range of operation of the pump.

When considering all tested combinations, Figure 8 identifies the component responsible for the operational bottleneck. The evaporator is the dominant limiting component, accounting for nearly 70% of the infeasible cases. Out of the 46,656 possible operating combinations evaluated, the developed off-design model achieved feasible operation in only 7.8% of cases, corresponding to 3,655 valid combinations. It is important to note that the order at which the integrated model progresses affects which component is identified during this analysis. For instance, for a given set of inputs, both the condenser and the pump could compromise the operation, but because the condenser is the first component to be tested, it is assumed to be the responsible for the operational bottleneck.

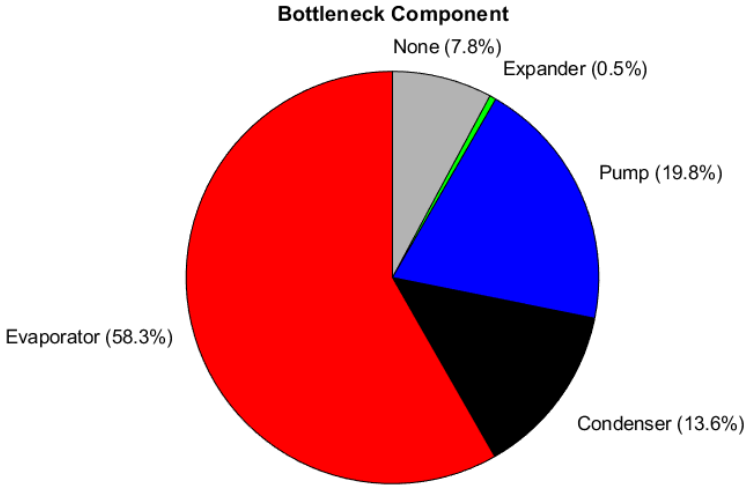

Figure. 8. *Responsible component for the bottleneck effect for all possible combinations tested.*

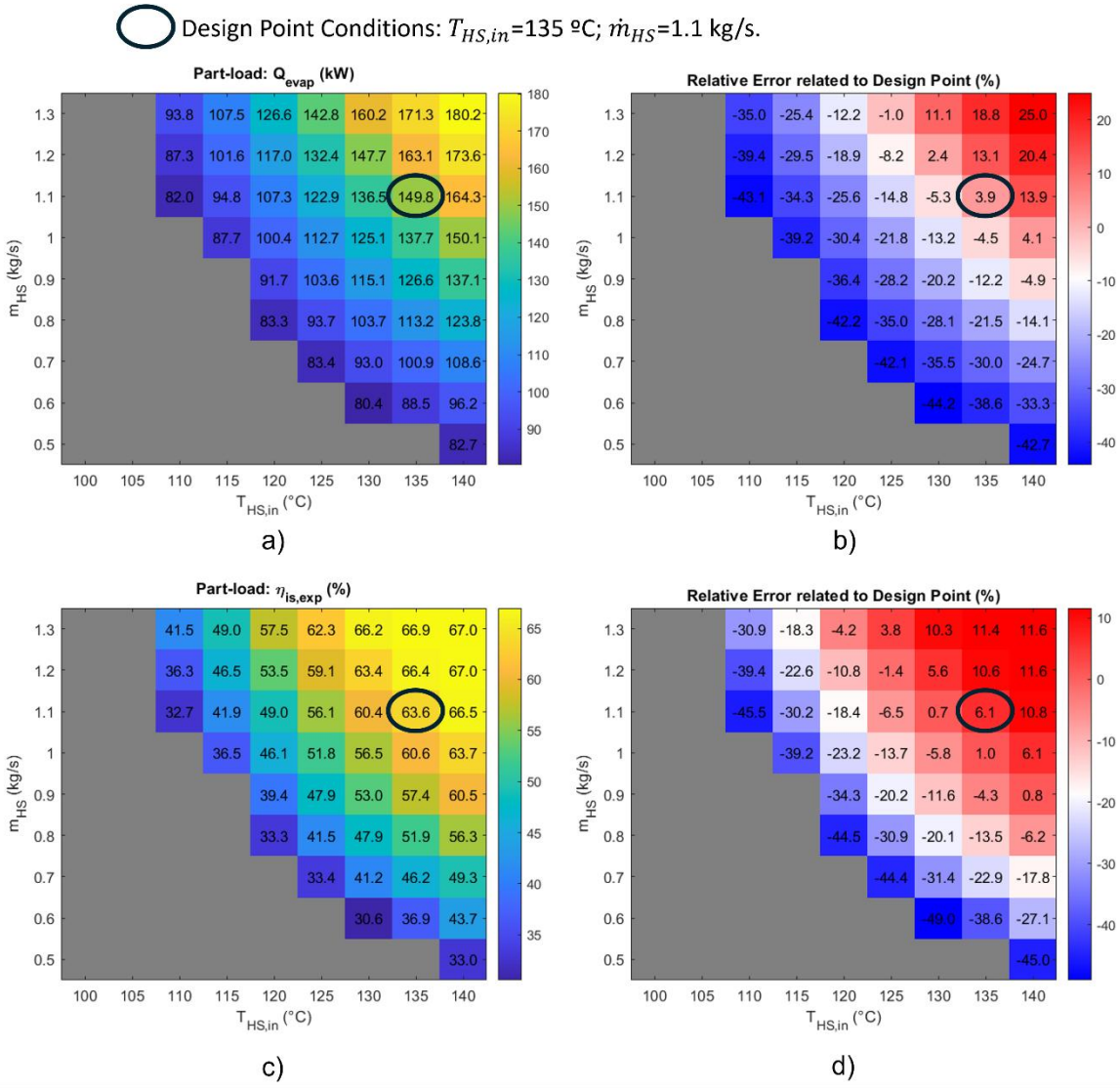

Figure. 9. *a) Part-load assessment of Q_{evap}, b) Relative error of Q_{evap} to the design-point, c) Part-load assessment of $\eta_{is,exp}$, b) Relative error of $\eta_{is,exp}$ to the design-point.*

While the off-design model operating in design point conditions resulted in a η_{ex} and η_{th} lower than the design model, in Figure 9, where the obtained Q_{evap} and $\eta_{is,exp}$ are presented for all heat source combinations, a different aspect is observed.
Under design conditions, the off-design model predicts higher values of both the thermal power supplied to the working fluid and the expander isentropic efficiency compared to the design model. While the design model assumes a fixed superheating degree of 5 ºC, the off-design model adopts a more flexible approach, allowing higher superheating levels, provided that the evaporator operates within its admissible limits.
As a result, under design-point conditions, the off-design model yields a superheating degree close to 10 ºC, along with a higher working fluid mass flow rate. This leads to an increase in the heat transferred in the evaporator Q_{evap} and a higher rotational speed of the expander, which in turn improves its isentropic efficiency and enhances the electrical power output.
However, the pump isentropic efficiency predicted by the off-design model is significantly lower than that assumed in the design model under the same conditions. This reduction leads to an increase in the pump work consumption. Consequently, the net power output W_{net} of the off-design model is lower, resulting in reduced exergy and thermal efficiencies.

5. Conclusions and future perspectives

In this work, an off-design model was developed by individually modelling each ORC component and subsequently integrating them into a unified system model, ensuring full thermodynamic closure of the cycle. The selected components were defined based on a design model corresponding to a specific design-point condition, characterized by the heat source inlet temperature and mass flow rate. The part-load performance of the system was evaluated by varying the heat source conditions and, for each combination, adjusting the working fluid mass flow rate and condensation pressure.
The results indicate that the off-design model predicts exergy and thermal efficiencies with relative deviations of 4.2% and 7.7%, respectively, compared to the design model under the same reference conditions. However, the system was only able to operate and generate electricity for 45 out of the 81 tested combinations of heat source inlet temperature and mass flow rate, with the evaporator identified as the primary limiting component.
Regarding component-level performance, the off-design model predicts higher heat transfer rates in the evaporator and improved expander isentropic efficiency when compared to the design model. Nevertheless, due to the overestimation of pump isentropic efficiency in the design model, the increase in expander work output is insufficient to offset the higher pump work consumption predicted by the off-design model, ultimately leading to a reduction in net power output.
For further validation of the proposed off-design model, future work should include experimental investigations to assess the accuracy and robustness of the modelling approach.

Acknowledgments

This research is financed by PRR - Recovery and Resilience Plan and by the Next Generation EU Funds, following NOTICE N.º 02/C05-i01/2022, Component 5 – Capitalization and Business Innovation - Mobilizing Agendas for Business Innovation under the AM2R project “Mobilizing Agenda for business innovation in the Two Wheels sector” (reference: 7253).

Nomenclature

A area, m$^{2)}$

b flow channel gap, m

Bo boiling number, -

BPHE brazed plate heat exchanger

Dh hydraulic diameter

$\dot{E}$ exergy flow rate

Exp expander

h specific enthalpy, kJ/kg

LMTD logarithmic mean temperature difference

Lp effective plate length, m

Lw effective plate height, m

$\dot{m}$ mass flow rate, kg/s

Npl number of plates

$Nrot$ rotational speed, rpm

ORC organic Rankine cycle
P power, kW
p pressure, kPa
P_C corrugation pitch, m
Pr Prandtl number, -
$\dot{Q}$ thermal load (kW)
Re Reynolds number, -
RP pressure ratio, -
s specific entropy, kJ/(kg.K)
T temperature, ºC
$\dot{W}$ mechanical work, kW
WHR waste heat recovery

Greek symbols

β Chevron angle
η efficiency
φ enlargement factor

Subscripts and superscripts

0 reference conditions
$cond$ condenser
CS cold sink
eff effective
$elect$ electrical
ex exergy
exp expander
$geom$ geometry
HS heat source
in inlet
$init$ initial
is isentropic
out outlet
$proj$ projected
SH superheating
th thermodynamic
WF working fluid

References

1. Loni, R.; Najafi, G.; Bellos, E.; Rajaee, F.; Said, Z.; Mazlan, M. A Review of Industrial Waste Heat Recovery System for Power Generation with Organic Rankine Cycle: Recent Challenges and Future Outlook. *J. Clean. Prod.* **2021**, *287*, 125070, doi:10.1016/j.jclepro.2020.125070.

2. Tchanche, B.F.; Lambrinos, Gr.; Frangoudakis, A.; Papadakis, G. Low-Grade Heat Conversion into Power Using Organic Rankine Cycles – A Review of Various Applications. *Renewable and Sustainable En ergy Reviews* **2011**, *15*, 3963–3979, doi:10.1016/j.rser.2011.07.024.

3. Hung, T.C.; Shai, T.Y.; Wang, S.K. A Review of Organic Rankine Cycles (ORCs) for the Recovery of Low-Grade Waste Heat. *Energy* **1997**, *22*, 661–667, doi:10.1016/S0360-5442(96)00165-X.

4. Wang, D.; Ling, X.; Peng, H.; Liu, L.; Tao, L. Efficiency and Optimal Performance Evaluation of Organic Rankine Cycle for Low Grade Waste Heat Power Generation. *Energy* **2013**, *50*, 343–352, doi:10.1016/j.energy.2012.11.010.

5. Santos, M.; André, J.; Mendes, R.; Ribeiro, J.B. General Framework for Hermetic Scroll Expander Modelling Derived from Commercial Compressor. *Appl. Therm. Eng.* **2025**, *271*, 126314, doi:10.1016/J.APPLTHERMALENG.2025.126314.

6. Wieland, C.; Schifflechner, C.; Braimakis, K.; Kaufmann, F.; Dawo, F.; Karellas, S.; Besagni, G.; Markides, C.N. Innovations for Organic Rankine Cycle Power Systems: Current Trends and Future Perspectives. *Appl. Therm. Eng.* **2023**, *225*, 120201, doi:10.1016/J.APPLTHERMALENG.2023.120201.

7. Santos, M.; André, J.; Francisco, S.; Mendes, R.; Ribeiro, J. Off-Design Modelling of an Organic Rankine Cycle Micro-CHP: Modular Framework, Calibration and Validation. *Appl. Therm. Eng.* **2018**, *137*, 848–867, doi:https://doi.org/10.1016/j.applthermaleng.2018.04.009.

8. Chatzopoulou, M.A.; Lecompte, S.; Paepe, M. De; Markides, C.N. Off-Design Optimisation of Organic Rankine Cycle (ORC) Engines with Different Heat Exchangers and Volumetric Expanders in Waste Heat Recovery Applications. *Appl. Energy* **2019**, *253*, 113442, doi:10.1016/J.APENERGY.2019.113442.

9. Wang, L.; Bu, X.; Li, H. Multi-Objective Optimization and off-Design Evaluation of Organic Rankine Cycle (ORC) for Low-Grade Waste Heat Recovery. *Energy* **2020**, *203*, 117809, doi:10.1016/J.ENERGY.2020.117809.

10. Lemort, V.; Quoilin, S.; Cuevas, C.; Lebrun, J. Testing and Modeling a Scroll Expander Integrated into an Organic Rankine Cycle. *Appl. Therm. Eng.* **2009**, *29*, 3094–3102, doi:10.1016/J.APPLTHERMALENG.2009.04.013.

11. Quoilin, S.; Lemort, V.; Lebrun, J. Experimental Study and Modeling of an Organic Rankine Cycle Using Scroll Expander. *Appl. Energy* **2010**, *87*, 1260–1268, doi:10.1016/J.APENERGY.2009.06.026.

12. Declaye, S.; Quoilin, S.; Guillaume, L.; Lemort, V. Experimental Study on an Open-Drive Scroll Expander Integrated into an ORC (Organic Rankine Cycle) System with R245fa as Working Fluid. *Energy* **2013**, *55*, 173–183, doi:10.1016/J.ENERGY.2013.04.003.

13. Martin, H. A Theoretical Approach to Predict the Performance of Chevron-Type Plate Heat Exchangers. *Chemical Engineering and Processing: Process Intensification* **1996**, *35*, 301–310, doi:https://doi.org/10.1016/0255-2701(95)04129-X.

14. Dickes, R.; Dumont, O.; Guillaume, L.; Quoilin, S.; Lemort, V. Charge-Sensitive Modelling of Organic Rankine Cycle Power Systems for off-Design Performance Simulation. *Appl. Energy* **2018**, *212*, 1262–1281, doi:10.1016/J.APENERGY.2018.01.004.

15. Han, D.-H.; Lee, K.-J.; Kim, Y.-H. The Characteristics of Condensation in Brazed Plate Heat Exchangers with Different Chevron Angles. *Journal- Korean Physical Society* **2003**, *43*, 66–73.

16. Han, D.H.; Lee, K.J.; Kim, Y.H. Experiments on the Characteristics of Evaporation of R410A in Brazed Plate Heat Exchangers with Different Geometric Configurations. *Appl. Therm. Eng.* **2003**, *23*, 1209–1225, doi:10.1016/S1359-4311(03)00061-9.

17. Jo, C.U.; Lee, D.C.; Chung, H.J.; Kang, Y.; Kim, Y. Comparative Evaluation of the Evaporation Heat Transfer Characteristics of a Low-GWP Refrigerant R-1234ze(E) between Shell-and-Plate and Plate Heat Exchangers. *Int. J. Heat Mass Transf.* **2020**, *153*, 119598, doi:10.1016/J.IJHEATMASSTRANSFER.2020.119598.

18. Calli, O.; Colpan, C.O.; Gunerhan, H. Thermal Modelling of a Plate-Type Heat Exchanger-Based Biomass-Fired Regenerative Organic Rankine Cycle. In *The Role of Exergy in Energy and the Environment*; Nižetić, S., Papadopoulos, A., Eds.; Springer International Publishing: Cham, 2018; pp. 189–203 ISBN 978-3-319-89845-2.